(2)

Semi-Annual Report

Low Temperature Deposition and Characterization of N- and P-Type Silicon Carbide Thin Films and Associated Ohmic and Schottky Contacts

Supported under Grant #N00014-92-J-1500
Office of the Chief of Naval Research
Report for the period January 1, 1993–June 30, 1993

R. F. Davis and R. J. Nemanich*
M. C. Benjamin, R. S. Kern, R. Patterson,
L. Spellman-Porter, and S. Tanaka
Materials Science and Engineering Department
*Department of Physics
North Carolina State University
Raleigh, NC 27695

June, 1993

REPORT DOCUMENTATION PAGE

Form Approved
OMB No. 0704-0188

1. AGENCY USE ONLY (Leave blank)	2. REPORT DATE	3. REPORT TYPE AND DATES COVERED
	June, 1993	Semi-Annual 1/1/93–6/30/93

4. TITLE AND SUBTITLE
Low Temperature Deposition and Characterization of N- and P-Type Silicon Carbide Thin Films and Associated Ohmic and Schottky Contacts

5. FUNDING NUMBERS
sic0002---02
1261
N00179
N66005
4B855

6. AUTHOR(S)
Robert F. Davis

7. PERFORMING ORGANIZATION NAME(S) AND ADDRESS(ES)
North Carolina State University
Hillsborough Street
Raleigh, NC 27695

8. PERFORMING ORGANIZATION REPORT NUMBER
N00014-92-J-1500

9. SPONSORING/MONITORING AGENCY NAMES(S) AND ADDRESS(ES)
Sponsoring: ONR, Code 1511:CLC, 800 N. Quincy, Arlington, VA 22217-5000
Monitoring: Office of Naval Research Resider
The Ohio State University Research Center
1960 Kenny Road
Columbus, OH 43210-1063

10. SPONSORING/MONITORING AGENCY REPORT NUMBER

11. SUPPLEMENTARY NOTES

12a. DISTRIBUTION/AVAILABILITY STATEMENT
Approved for Public Release; Distribution Unlimited

12b. DISTRIBUTION CODE

13. ABSTRACT *(Maximum 200 words)*

Monocrystalline films of SiC were grown on α(6H)-SiC(0001) wafers using disilane (Si_2H_6) and ethylene (C_2H_4) by gas-source MBE at 1050°C. The nucleation and growth of cubic β-SiC(111) on the surface terraces of the hexagonal 6H-SiC rather than on the step surfaces and the resultant formation of double positioning boundaries is discussed. The reconfiguration of the growth system leading to enhanced control over polytype deposition is also described. Thin film contacts of Ti, Pt, Hf, and Co were deposited in UHV onto unheated, n-type vicinal α(6H)-SiC(0001) films by electron beam evaporation. All as-deposited contacts were rectifying with low ideality factors ($n<1.1$), low leakage currents and Schottky barrier heights between 0.85 eV and 1.15 eV. The lowest leakage currents were $<5\times10^{-8}$ A/cm^2 at –10 V. Titanium and Pt remained relatively stable after annealing at 700–750°C; whereas, Co became ohmic after annealing for two minutes at 1000°C. UV photoemission studies on both SiC/metal interfaces and the surface of AlN(0001) deposited on SiC have been initiated. A major emphasis is on surface cleanliness prior to metal deposition. A spectral feature observed in the AlN is attributed to the initial indication of negative electron affinity in this material. Chemical interdiffusion between α(6H)-SiC wafers and epitaxially deposited 2H-AlN films are under investigation within the temperature range of 1500°C to 1700°C. Scanning Auger spectroscopy and XTEM is being used to determine the diffusion profiles and the occurrence of new phases. The Auger data and electron energy loss measurements are in disagreement. Additional diffusion and segregation research is under way to resolve this conflict.

14. SUBJECT TERMS
SiC, AlN, gas source molecular beam epitaxy, transmission electron microscopy, metal contacts, Ti, Pt, Hf, Co, ideality factors, leakage currents, Schottky barrier heights, UV photoemission, negative electron affinity, chemical interdiffusion

15. NUMBER OF PAGES
34

16. PRICE CODE

17. SECURITY CLASSIFICATION OF REPORT	18. SECURITY CLASSIFICATION OF THIS PAGE	19. SECURITY CLASSIFICATION OF ABSTRACT	20. LIMITATION OF ABSTRACT
UNCLAS	UNCLAS	UNCLAS	SAR

DISCLAIMER NOTICE

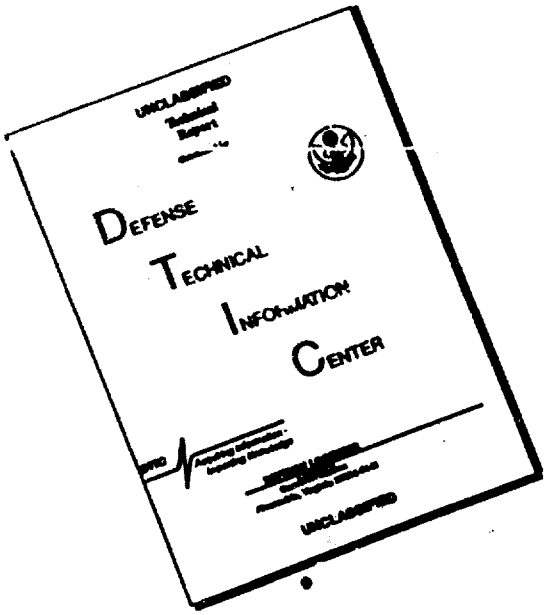

THIS DOCUMENT IS BEST QUALITY AVAILABLE. THE COPY FURNISHED TO DTIC CONTAINED A SIGNIFICANT NUMBER OF PAGES WHICH DO NOT REPRODUCE LEGIBLY.

Table of Contents

I. Introduction

Silicon carbide (SiC) is a wide bandgap material that exhibits polytypism, a one-dimensional polymorphism arising from the various possible stacking sequences of the silicon and carbon layers. The lone cubic polytype, β-SiC, crystallizes in the zincblende structure and is commonly referred to as 3C-SiC. In addition, there are also approximately 250 other rhombohedral and hexagonal polytypes [1] that are all classed under the heading of α-SiC. The most common of the α-SiC polytypes is 6H-SiC, where the 6 refers to the number of Si/C bilayers along the closest packed direction in the unit cell and the H indicates that the crystal structure is hexagonal.

Beta (3C)-SiC is of considerable interest for electronic applications that utilize its attractive physical and electronic properties such as wide bandgap (2.2 eV at 300K) [2], high breakdown electric field (2.5×10^6 V/cm) [3], high thermal conductivity (3.9 W/cm °C) [4], high melting point (3103K at 30 atm) [5], high saturated drift velocity (2×10^7 m/s) [6], and small dielectric constant (9.7) [7]. Primarily due to its higher electron mobility than that of the hexagonal polytypes, such as 6H-SiC [8], β-SiC remains preferable to hexagonal SiC for most device applications.

Most 3C-SiC thin film growth to date has been performed on Si substrates. Large-area, crack-free, and relatively thick (up to 30 μm) epitaxial 3C-SiC thin films have been grown on Si (100) by exposing the Si substrate to a C-bearing gaseous species prior to further SiC growth [7, 9, 10]. However, these films exhibited large numbers of line and planar defects due to large lattice and thermal mismatches between SiC and Si. One particular type of planar defect, the inversion domain boundary (IDB), was eliminated with the use of Si (100) substrates cut 2°–4° toward [011] [11–13]. Growth on Si substrates has allowed much understanding of SiC growth processes and device development to occur, but the large thermal and lattice mismatches between SiC and Si hamper further development using Si substrates. As a result, great effort has been made to develop methods for growth SiC single crystal substrates for homoepitaxial growth of SiC thin films.

Since the 1950's, monocrystalline single crystals of 6H-SiC have been grown at using the Lely sublimation process [14]. However, nucleation was uncontrolled using this process and control of resultant polytypes was difficult. SiC single crystals inadvertently formed during the industrial Acheson process have also been used as substrates for SiC growth. However, neither these crystals or those formed using the Lely process are large enough for practical device applications. Recently, using a seeded sublimation-growth process, boules of single polytype 6H-SiC of > 1 inch diameter of much higher quality of that obtained using the Lely process have been grown. The use of single crystals of the 6H polytype cut from these boules has given a significant boost to SiC device development.

Silicon carbide epitaxial thin film growth on hexagonal SiC substrates has been reported since the 1960's. The use of nominally on-axis SiC substrates has usually resulted in growth of 3C-SiC films. Films of 3C-SiC (111) grown by CVD have been formed on 6H-SiC substrates less than 1° off (0001) [15]. Films of 3C-SiC on 6H-SiC substrates have typically had much lower defect densities than those grown on Si substrates. The major defects present in 3C-SiC/6H-SiC films have been double positioning boundaries (DPB) [16]. Despite the presence of DPBs, the resultant material was of sufficient quality to further device development of SiC. The use of off-axis 6H-SiC (0001) substrates has resulted in growth of high-quality monocrystalline 6H-SiC layers with very low defect densities [17].

In addition, the use of more advanced deposition techniques, such as molecular beam epitaxy (MBE), has been reported for SiC in order to reduce the growth temperature and from about 1400–1500°C on 6H-SiC substrates. Si and C electron-beam sources have been used to epitaxially deposit SiC on 6H-SiC (0001) at temperatures of 1150°C [18]. Ion-beam deposition of epitaxial 3C-SiC on 6H-SiC has also been obtained at the temperature of 750°C using mass-separated ion beams of $^{30}Si^{+}$ and $^{13}C^{+}$ [19].

Aluminum nitride (AlN) is also of particular interest at this time because of its very large bandgap. It is the only intermediate phase in the Al-N system and normally forms in the wurtzite (2H-AlN) structure. Most current uses of AlN center on its mechanical properties, such as high hardness (9 on Mohs scale), chemical stability, and decomposition temperature of about 2000°C [20]. Properties such as high electrical resistivity (typically $\geq 10^{13}$ Ω-cm), high thermal conductivity (3.2 W/cm K) [21], and low dielectric constant ($\varepsilon \approx 9.0$) make it useful as a potential substrate material for semiconductor devices as well as for heat sinks. The wurtzite form has a bandgap of 6.28 eV [22] and is a direct transition, thus it is of great interest for optoelectronic applications in the ultraviolet region.

Because of the difference in bandgaps (2.28 eV for 3C-SiC and 6.28 eV for 2H-AlN) between the materials, a considerable range of wide bandgap materials, made with these materials, should be possible. Two procedures for bandgap engineering are solid solutions and multilayers. A particularly important factor is that the two materials have a lattice mismatch of less than one percent.

Research in ceramic systems suggests that complete solid solubility of AlN in SiC may exist [23]. Solid solutions of the wurtzite crystal structure should have E_g from 3.33 eV to 6.28 eV at 0 K. Although it has not been measured, the bandgap of cubic AlN has been estimated to be around 5.11 eV at absolute zero and is believed to be indirect [24]. Cubic solid solutions should thus have E_g from 2.28 eV to roughly 5.11 eV at 0 K and would be indirect at all compositions if theory holds true.

Because of their similarity in structure and close lattice and thermal match, AlN-SiC heterostructures are feasible for electronic and optoelectronic devices in the blue and infrared

region. Monocrystalline AlN layers have been formed by CVD on SiC substrates [25] and SiC layers have been formed on AlN substrates formed by AlN sputtering on single crystal W [26]. In addition, theory on electronic structure and bonding at SiC/AlN interfaces [24] exists and critical layer thicknesses for misfit dislocation formation have been calculated for cubic AlN/SiC [27]. Note that AlN (at least in the wurtzite structure) is a direct-gap material and SiC is an indirect gap material. Superlattices of these materials would have a different band structure than either constituent element. The Brillouin zone of a superlattice in the direction normal to the interfaces is reduced in size. This reduction in zone size relative to bulk semiconductors causes the superlattice bands to be "folded into" this new, smaller zone. This folding can cause certain superlattice states to occur at different points in k space than the corresponding bulk material states [28]. This can lead to direct transitions between materials which in the bulk form have indirect transitions. This has been demonstrated in the case of $GaAs_{0.4}P_{0.6}$/GaP and $GaAs_{0.2}P_{0.8}$/GaP superlattices, where both constituents are indirect in the bulk form [29]. Whether this is possible in the case of AlN/SiC is unknown, but very intriguing. It may be possible to obtain direct transitions throughout nearly the entire bandgap range with use of superlattices of AlN and SiC. Use of solid solutions in superlattices introduces additional degrees of freedom. For example, the bandgap can be varied independently of the lattice constant with proper choice of layer thickness and composition if superlattices of solid solutions of AlN and SiC were formed.

Due to the potential applications of solid solutions and superlattice structures of these two materials, an MBE/ALE system was commissioned, designed, and constructed for growth of the individual compounds of SiC and AlN, as well as solid solutions and heterostructures of these two materials. Dithisimal studies concerned with the kinetics and mechanisms of mass transport of Si, C, Al and N at the SiC/AlN interface are also being conducted in tandem with the deposition investigations.

A very important additional goal of this research is to understand what controls the contact electrical characteristics of specific metals to n-type 6H-SiC and to use this information to form good ohmic and Schottky contacts. A list of five metals to be studied, which consists of Ti, Pt, Hf, Co, and Sr, was created at the beginning of this research project. The selection process began by taking the simplest case, an ideal contact which behaves according to Schottky-Mott theory. This theory proposes that when an intimate metal-semiconductor contact is made the Fermi levels align, creating an energy barrier equal to the difference between the workfunction of the metal and the electron affinity of the semiconductor. It is the height of this barrier which determines how the contact will behave; for ohmic contacts it is desirable to have either no barrier or a negative barrier to electron flow, while for a good Schottky contact a large barrier is desired.

Although metals were chosen optimistically, i.e. on the basis that they will form ideal contacts, some evidence exists that the contact properties will be more complicated. J. Pelletier *et al.* [30] have reported Fermi level pinning in 6H-SiC due to intrinsic surface states, suggesting little dependence of barrier height on the workfunction of the metal. In addition, L. J. Brillson [31, 32] predicts the pinning rate to be higher for more covalently bonded materials. Other complications may arise if the surface is not chemically pristine. A major part of this project will be devoted to determining whether the contacts behave at all ideally, and if not, whether the Fermi level is pinned by intrinsic or extrinsic effects.

Along with examining the barriers of the pure metal contacts, the chemistry upon annealing will be studied and correlated with the resulting electrical behavior. The electrical behavior will be quantified both macroscopically in terms of current-voltage characteristics and microscopically in terms of barrier height. Identification of the phases formed will present the opportunity to attribute the electrical characteristics to the new phase in contact with silicon carbide.

Within this reporting period, monocrystalline films of SiC have been grown on α(6H)-SiC (0001) using disilane (Si_2H_6) and ethylene (C_2H_4) by gas-source molecular beam epitaxy at 1050°C. Moreover, this growth system has been reconfigured to ensure enhanced SiC polotype control of the deposited film. Titanium, Pt, Hf and Co rectifying contacts with low ideality factors (< 1.1) and low leakage currents (< 5×10^{-8}A/cm^2) and barrier heights between 0.85 eV and 1.15 eV have been deposited. Co and Pt ohmic contacts are also under study. UV photoemission is also being conducted on these metal/SiC interfaces and on the AlN (0001) surface. The reason for the latter study is to determine the negative electron affinity character of this surface. Finally, chemical interdiffusion studies between AlN and SiC are being conducted to determine if solid solutions do occur and their nature.

The experimental procedures, results, discussion of these results, conclusions and plans for future efforts for each of the topics noted above are presented in the following sections. Each of these sections is self-contained with its own figures, tables and references.

References

1. G. R. Fisher and P. Barnes, Philos. Mag. B **61**, 217 (1990).
2. H. P. Philipp and E. A. Taft, in *Silicon Carbide, A High Temperature Semiconductor*, edited by J. R. O'Connor and J. Smiltens (Pergamon, New York, 1960), p. 371.
3. W. von Muench and I. Pfaffender, J. Appl. Phys. **48**, 4831 (1977).
4. E. A. Bergemeister, W. von Muench, and E. Pettenpaul, J. Appl. Phys. **50**, 5790 (1974).
5. R. I. Skace and G. A. Slack, in *Silicon Carbide, A High Temperature Semiconductor*, edited by J. R. O'Connor and J. Smiltens (Pergamon, New York, 1960), p. 24.
6. W. von Muench and E. Pettenpaul, J. Appl. Phys. **48**, 4823 (1977).
7. S. Nishino, Y. Hazuki, H. Matsunami, and T. Tanaka, J. Electrochem Soc. **127**, 2674 (1980).

8. P. Das and K. Ferry, Solid State Electronics **19**, 851 (1976).
9. K. Sasaki, E. Sakuma, S. Misawa, S. Yoshida, and S. Gonda, Appl. Phys. Lett. **45**, 72 (1984).
10. P. Liaw and R. F. Davis, J. Electrochem. Soc. **132**, 642 (1985).
11. K. Shibahara, S. Nishino, and H. Matsunami, J. Cryst. Growth **78**, 538 (1986).
12. J. A. Powell, L. G. Matus, M. A. Kuczmarski, C. M. Chorey, T. T. Cheng, and P. Pirouz, Appl. Phys. Lett. **51**, 823 (1987).
13. H. S. Kong, Y. C. Wang, J. T. Glass, and R. F. Davis, J. Mater. Res **3**, 521 (1988).
14. J. A. Lely, Ber. Deut. Keram. Ges. **32**, 229 (1955).
15. H. S. Kong, J. T. Glass, and R. F. Davis, Appl. Phys. Lett. **49**, 1074 (1986).
16. H. S. Kong, B. L. Jiang, J. T. Glass, G. A. Rozgonyi, and K. L. More, J. Appl. Phys. **63**, 2645 (1988).
17. H. S. Kong, J. T. Glass, and R. F. Davis, J. Appl. Phys. **64**, 2672 (1988).
18. S. Kaneda, Y. Sakamoto, T. Mihara, and T. Tanaka, J. Cryst. Growth **81**, 536 (1987).
19. S. P. Withrow, K. L. More, R. A. Zuhr, and T. E. Haynes, Vacuum **39**, 1065 (1990).
20. C. F. Cline and J. S. Kahn, J. Electrochem. Soc, **110**, 773 (1963).
21. G. A. Slack, J. Phys. Chem. Solids **34**, 321 (1973).
22. W. M. Yim, E. J. Stofko, P. J. Zanzucci, J. I. Pankove, M. Ettenberg, and S. L. Gilbert, J. Appl. Phys. **44**, 292 (1973).
23. See, for example, R. Ruh and A. Zangvil, J. Am. Ceram. Soc. **65**, 260 (1982).
24. W. R. L. Lambrecht and B. Segall, Phys. Rev. B **43**, 7070 (1991).
25. T. L. Chu, D. W. Ing, and A. J. Norieka, Solid-State Electron. **10**, 1023 (1967).
26. R. F. Rutz and J. J. Cuomo, in *Silicon Carbide-1973*, ed. by R. C. Marshall, J. W. Faust, Jr., and C. E. Ryan, Univ. of South Carolina Press, Columbia, p. 72 (1974).
27. M. E. Sherwin and T. J. Drummond, J. Appl. Phys. **69**, 8423 (1991).
28. G. C. Osbourn, J. Vac. Sci. Technol. B **1**, 379 (1983).
29. P. L. Gourley, R. M. Biefeld, G. C. Osbourn, and I. J. Fritz, *Proceedings of 1982 Int'l Symposium on GaAs and Related Compounds* (Institute of Physics, Berkshire, 1983), p. 248.
30. J. Pelletier, D. Gervais, and C. Pomot, J. Appl. **55**, 994 (1984).
31. L. J. Brillson, Phys. Rev. B **18**, 2431 (1978).
32. L. J. Brillson, Surf. Sci. Rep. **2**, 123 (1982).

II. Growth of Doped and Undoped SiC by Gas-source Molecular Beam Epitaxy

A. Introduction

The use of more advanced deposition techniques, such as molecular beam epitaxy (MBE), has been reported for the deposition of SiC thin films in order to reduce the growth temperature from that used in chemical vapor deposition (1450–1600 °C) on 6H-SiC substrates. Silicon and C electron-beam sources have been used to epitaxially deposit SiC on 6H-SiC (0001) at temperatures of 1150 °C [1]. Ion-beam deposition of epitaxial 3C-SiC on 6H-SiC has also been obtained at 750°C using mass-separated ion beams of $^{30}Si^{+}$ and $^{13}C^{+}$ [2]. In the present research program, a specially configured gas-source MBE is being employed to deposit undoped as well as n- and p-type SiC films. The procedures, results and a discussion of these results are presented in the following sections.

B. Experimental Procedure

Thin, epitaxial films of SiC were grown on the Si and C faces of 6H-SiC (0001) substrates supplied by Cree Research, Inc. These vicinal 6H-SiC (0001) wafers oriented 3-4° towards [11$\bar{2}$0] contained a 0.8 μm epitaxial 6H-SiC layer deposited via CVD and a thermally oxidized 50 nm layer to aid in wafer cleaning. Substrates were chemically cleaned prior to growth in a 10% HF solution for five minutes to remove the oxide, immediately loaded into the growth system and heated for five minutes at the growth temperature of 1050 °C.

All growth experiments were carried out in the gas-source molecular beam epitaxy system detailed in previous reports. The sources of Si and C were Si_2H_6 and C_2H_4 (both 99.99% pure), respectively. Dopant sources, Al for p-type and N for n-type, were solid Al (99.999% pure) evaporated from a standard MBE effusion cell and electron cyclotron resonance decomposed N_2 (99.9995% pure). Typical base pressures of 10^{-9} Torr were used. The growth rate of SiC was on the order of 60 Å h^{-1} when flow rates of 0.1 sccm (Si_2H_6) and 0.2 sccm (C_2H_4) were used.

Reflection high-energy electron diffraction (RHEED) at 10 kV and high-resolution transmission electron microscopy (HRTEM) were used for structure and microstructure analyses. Samples were prepared for HRTEM using standard techniques [3]. An Akashi EM 002B high-resolution transmission electron microscope was used at 200 kV for the HRTEM analysis.

C. Results and Discussion

Doped and undoped films have, to this point, resulted in monocrystalline, epitaxial layers of SiC. However, the layers have had rough surfaces and the appearance of three-dimensional

growth originating at the terraces of the vicinal substrates. This is shown in Fig. 1. Similar results have been obtained by Rowland *et al.* [4]. The resulting films are generally cubic (3c or β) SiC and have double positioning boundaries as evidenced by the RHEED (Fig. 2).

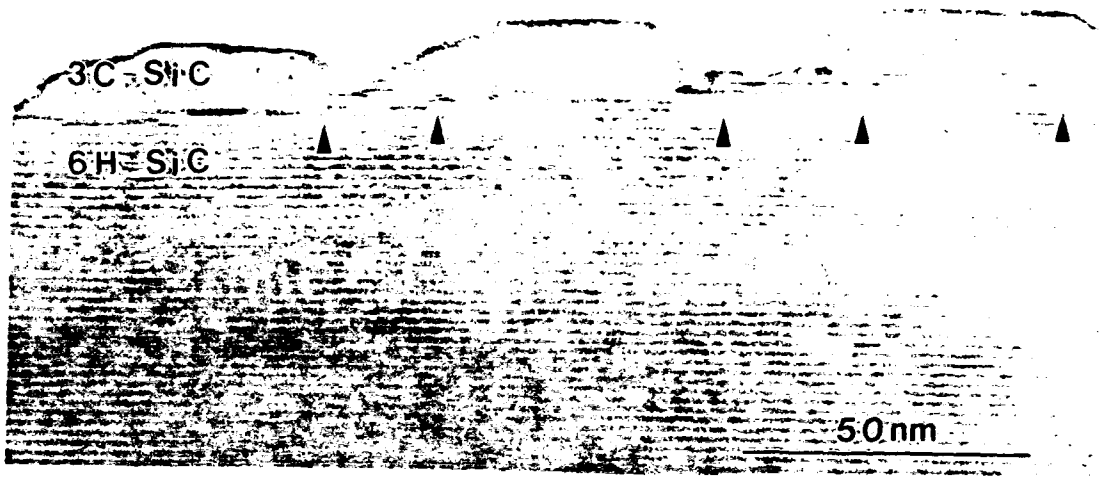

Figure 1. Cubic SiC layer grown on off-axis α(6H)-SiC indicating the preference to nucleate and grow on terraces.

Figure 2. RHEED image of a β-SiC layer ([110] azimuth) grown on off-axis α(6H)-SiC.

The double positioning boundaries (aka incoherent twin boundaries) noted above occur when 3C-SiC (111) is grown on Si (111) [5] or on-axis 6H-SiC [6] because two different

orientations, rotated 60° from each other, are present which have close-packed directions aligned in the interface. These orientations differ in the cubic stacking sequence, as one orientation has an ···ABCABC··· stacking sequence and the other has an ···ACBACB··· stacking sequence. Extra reflections in the [110] RHEED pattern due to double positioning twins would either coincide with those of the film or be displaced by 1/3[111]. An equivalent interpretation of the RHEED pattern is of two interpenetrating [110] RHEED patterns with a misorientation of 180°. This misorientation is caused by reflections from regions with both ···ABCABC··· and ···ACBACB··· sequences.

Figure 3 shows a wurtzitic (2H) SiC layer grown under identical conditions to the 3C-SiC layer shown in Fig. 1. The exact reason(s) for the growth of the 2H polytype (Eg = 3.3 eV) are not known at this time, but are believed to be a result of pretreatment of the substrate.

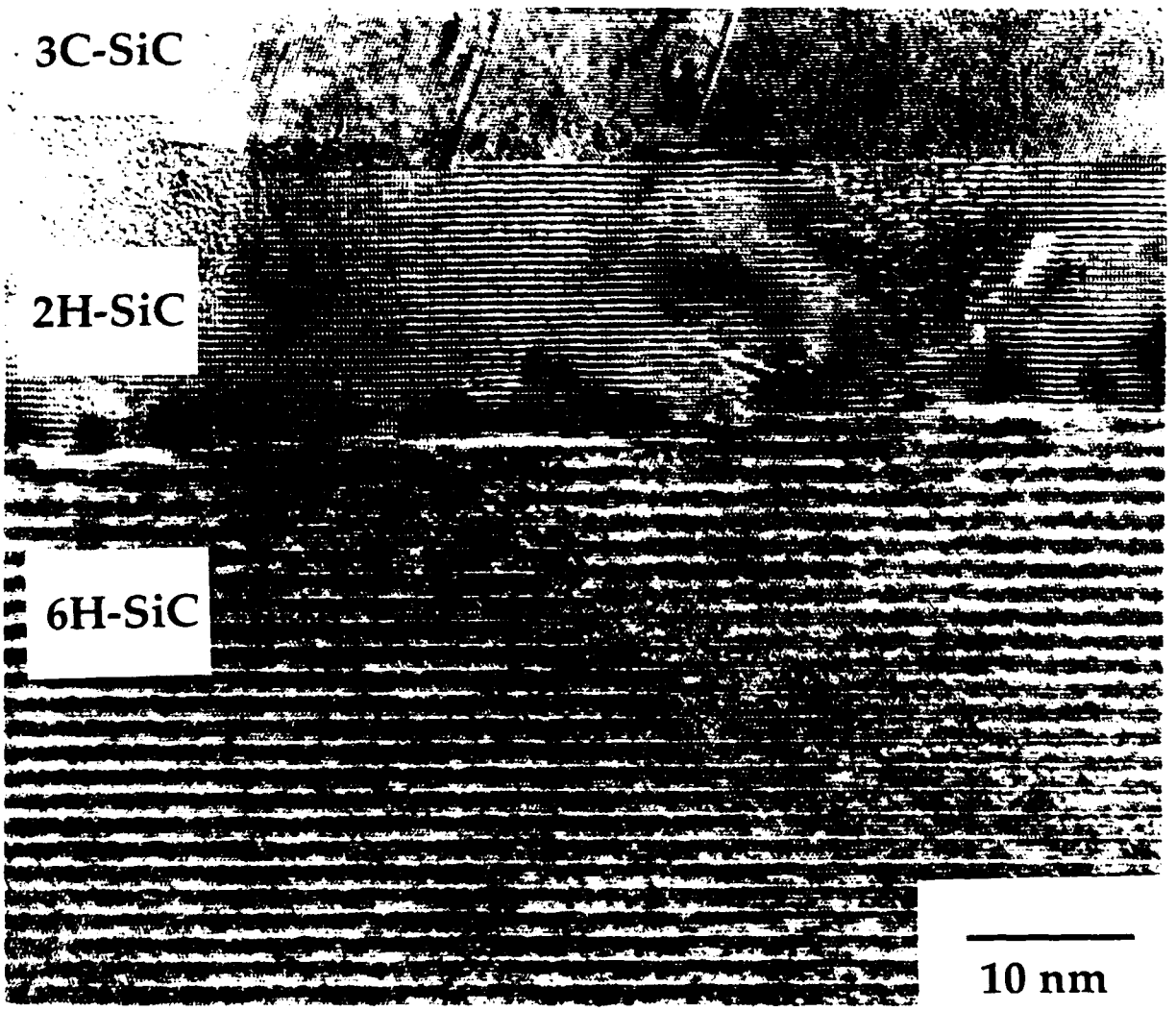

Figure 3. Wurtzitic (2H) SiC on 6H-SiC expected to be the result of wafer pretreatment.

Knippenberg [7] has postulated that the 2H polytype is a low temperature (1300–1600 °C) equilibrium form and Tairov and Tsvetkov [8] have suggested that this polytype is the only polytype that possesses a Si/C stoichiometry of 1.0.

D. Conclusions

The results shown in Figs. 1–3 indicate that the processing temperature is not sufficient to create uniform layers with sufficient atomic mobility to originate at the steps of the vicinal wafers rather than the terraces. Auger electron spectra and depth profiling displayed in previous reports confirms the formation of nominally stoichiometric SiC single crystal films.

E. Future Research Plans and Goals

A new heating element, manufactured by Advanced Ceramics, Inc., made of a composite graphite/boron nitride has been installed to replace the previously used tungsten filament. The new element, rated at T_{max} = 2500 °C, should allow for the higher temperatures desired for growth and controlled of doped and undoped SiC layers of superior quality. The 2H-SiC layer is presently attributed to a change in surface conditions during an initial heat treatment that this new heater can routinely perform. Additionally, a RHEED oscillation and in situ monitoring system has been purchased and is presently being used to monitor the pre-deposition and initial deposition effects of temperature, cleaning procedure and reactant introduction on polytype and film quality.

F. References

1. S. Kaneda, Y. Sakamoto, T. Mihara, and T. Tanaka, J. Cryst. Growth **81**, 536 (1987).
2. S. P. Withrow, K. L. More, R. A. Zuhr, and T. E. Haynes, Vacuum **39**, 1065 (1990).
3. J. C. Bravman and R. Sinclair, J. Electron Microsc. Tech. **1**, 53 (1987).
4. L. B. Rowland, R. S. Kern, S. Tanaka, and R. F. Davis, Appl. Phys. Lett., to be published.
5. I. H. Khan and R. N. Summergrad, Appl. Phys. Lett. **11**, 12 (1967).
6. H. S. Kong, B. L. Jiang, J. T. Glass, G. A. Rozgonyi, and K. L. More, J. Appl. Phys. **63**, 2645 (1988).
7. W. F. Knippenberg, Philips Res. Rep. **18**, 161 (1963).
8. Yu M. Tairov and V. F. Tsvetkov, in *Progress of Crystal Growth and Characterization, Vol. 7–Crystal Growth and Characterization of Polytype Structures*, edited by P. Krishna (Pergamon, New York, 1983), p. 111.

III. Ohmic and Schottky Contacts to n-type Alpha (6H) Silicon Carbide

A. Introduction

Metal-semiconductor interfaces are critical components of any electronic device. For efficient operation of electronic devices, it is necessary to fabricate both rectifying contacts with low leakage currents and ohmic contacts with low contact resistance. These characteristics require high and low Schottky barrier heights (SBH), respectively.

Although SiC devices have been used for high-power, -temperature, -speed, -frequency, radiation hard, and opto-electronic applications for several years, little is known about the science of controlling metal/SiC contact properties. In this research project several metal/SiC systems are being studied in terms of interfacial chemistry, structure, and electronics. This report discusses electrical properties and high resolution transmission electron microscopy results of four metal contacts before and after annealing.

B. Experimental Procedure

Vicinal single crystal, nitrogen-doped, n-type (~10^{18} cm^{-3}) substrates of 6H-SiC containing 0.5–0.8 μm thick, nitrogen-doped (~10^{16} cm^{-3} unless otherwise noted) homo-epitaxial films were provided by Cree Research, Inc. The Si-terminated (0001) surface, tilted 3°–4° towards [11$\bar{2}$0] was used for all depositions and analyses.

The substrate surfaces were cleaned in sequence using a 10 min. dip in either 10% HF in deionized water or a (10:1:1) solution of ethanol / HF / H_2O followed by a 15 min. thermal desorption at 700°C in ultra-high vacuum (UHV). The metals were deposited on chemically cleaned, unheated substrates by electron beam evaporation (base pressure < 2×10^{-10} Torr). For films less than or equal to ~10 nm, a deposition rate of ~1 nm/min. was used. For thicker films the rate was increased to ~2 nm/min. after deposition of the first 10 nm.

For electrical characterization the metals were deposited through a Mo mask in contact with the SiC surface, leaving a patterned metal film. Schottky diodes were fabricated using a mask with 500 μm and 750 μm diameter holes. A large area backside contact served as the ohmic contact.

For the purpose of measuring the specific contact resistance of ohmic contacts, the metal was deposited through a different Mo mask. In this case the epitaxial SiC layer had a carrier concentration of ~10^{18} cm^{-3}. The design of the mask follows the Transmission Line Model (TLM) discussed by Berger [1]. The contact resistance is calculated by comparing the total resistances between contacts of various separations.

Current-voltage (I–V) measurements were taken with a Rucker & Kolls Model 260 probe station in conjunction with an HP 4145A Semiconductor Parameter Analyzer. Capacitance-

voltage (C–V) measurements were taken at a frequency of 1 MHz with a Keithley 590 CV Analyzer.

All metal/SiC samples were prepared in cross-section for TEM analysis. High resolution images were obtained with an ISI EM 002B operating at 200 kV. Analytical electron microscopy was performed with a Philips 400 FEG, installed with Gatan 607 parallel electron energy loss spectrometer, operated at 100kV.

C. Results

Results of Ti, Pt, and Hf contacts have been reported [2], a summary of which will be presented in sections A, B, and C. Section D will discuss the most recent results. All contact metals, as-deposited at room temperature on n-type 6H-SiC, were rectifying with low ideality factors ($n<1.09$) and low leakage currents. Most of the differences in electrical properties, chemistry, and microstructure developed after annealing. Comparisons of the similarities and differences will be presented in the 'Discussion' section.

Ti Contacts. The room temperature deposition of Ti on (0001) SiC resulted in epitaxial films which were pseudomorphic with the substrate [3]. Both Ti (a=2.95 Å, c=4.68 Å) and 6H-SiC (a=3.08 Å, c=15.11 Å) have hexagonal crystal structures, corresponding to a 4% lattice mismatch in the (0001) basal plane.

Current-voltage measurements of these contacts showed rectifying behavior with typical leakage currents of 5×10^{-7} A/cm^2 at –10 V and resulted in a calculated Schottky barrier height of 0.85 eV. In comparison, the SBH calculated from C–V measurements was 0.88 eV. After annealing at 700°C for 20 minutes in UHV, the leakage increased; however, after further annealing for 60 minutes the characteristics in terms of leakage and ideality factors again improved.

Along with the changes in the electrical properties, annealing caused marked changes in the microstructure as observed from high resolution transmission electron microscopy (HRTEM). Figs. 1(a) and 1(b) show the phases which formed at the interfaces after annealing for 20 and 60 minutes, respectively. Both interfaces consist of a reaction zone approximately 15 nm thick with Ti_5Si_3 and a thin TiC layer extending across the SiC side of the interface. TiC particles in contact with the Ti phase disappeared after annealing for 60 min. Because TiC, which behaves electrically as a metal, is the only phase in contact with the SiC, it is this phase which is responsible for the electrical characteristics.

Pt Contacts. The electrical characteristics of Pt contacts before and after annealing were better than Ti in terms of leakage current and SBH. The leakage at –10 V was typically 5×10^{-8} A/cm^2, and the calculated SBH is 1.06 eV.

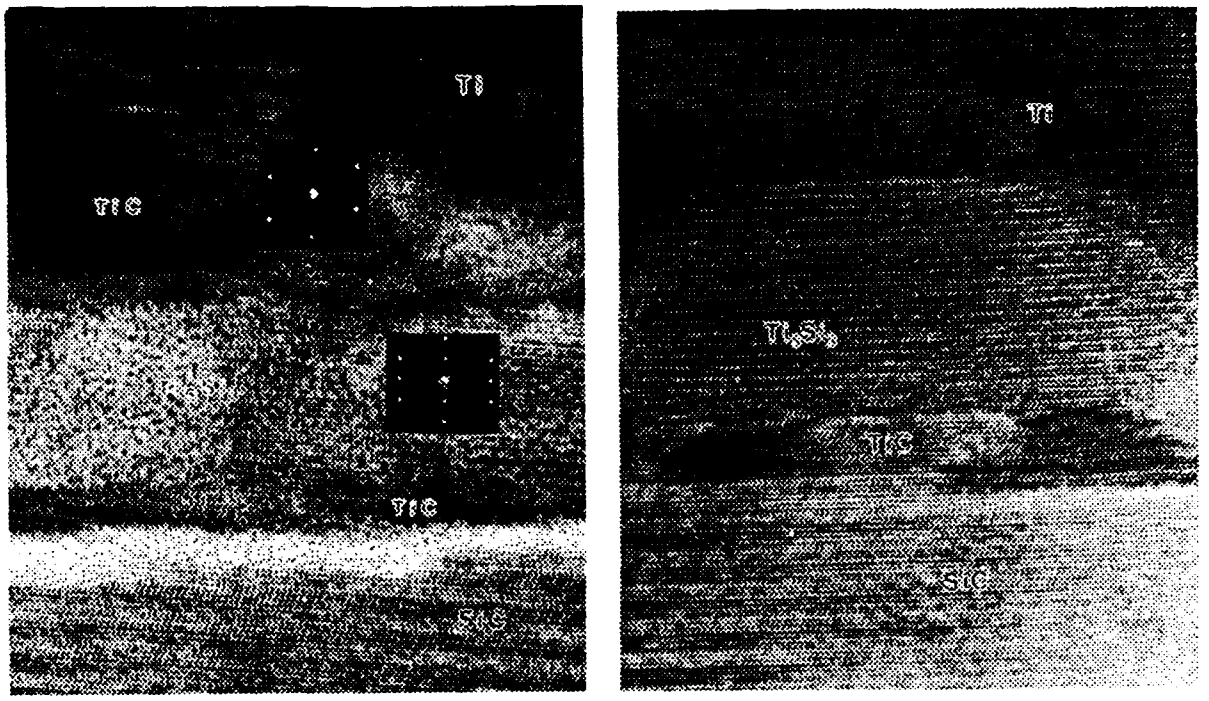

(a) (b)

Figure 1. HRTEM image of Ti/SiC after annealing at 700°C for (a) 20 min., (b) 60 min.

These contacts were UHV annealed from 450°C to 750°C in 100°C increments for 20 minutes at each temperature. The characteristics remained similar to those before annealing. Fig. 2 shows an interesting trend through this annealing series, throughout which the ideality factors and leakage currents remained low; the SBH increased with anneal temperature to 1.26 eV. These results are similar to those reported by Papanicolaou *et al.* [4] in which the SBH of Pt on β-SiC increased from 0.95 eV for as-deposited contacts to 1.35 eV after annealing at 800°C.

High resolution TEM analysis has been performed on both the as-deposited and annealed contacts. The as-deposited Pt film is polycrystalline with an average grain size of 10 ± 3 nm (Fig. 3). The thin amorphous layer visible at the interface and gradually disappearing in the thick regions, was attributed to oxygen-induced ion-milling damage. This trace oxygen was not detected in the annealed samples. After annealing at 750°C for 20 minutes, a pronounced reaction zone formed. The reaction zone (R.Z.) shown in Fig. 4 appears as dark crystalline and bright amorphous regions between the unreacted Pt and SiC. Electron energy loss spectroscopy (EELS) indicates that the amorphous phase contains both C and Pt. The dark crystalline phase was identified as Pt_2Si from optical digital diffraction patterns as well as micro-diffraction patterns. The platinum silicide, which is not completely separated from the Pt phase, is epitaxially related to the SiC substrate with $[11\bar{2}0]//(0001)$ and $[110]_{Pt_2Si}//(1\bar{1}00)_{SiC}$.

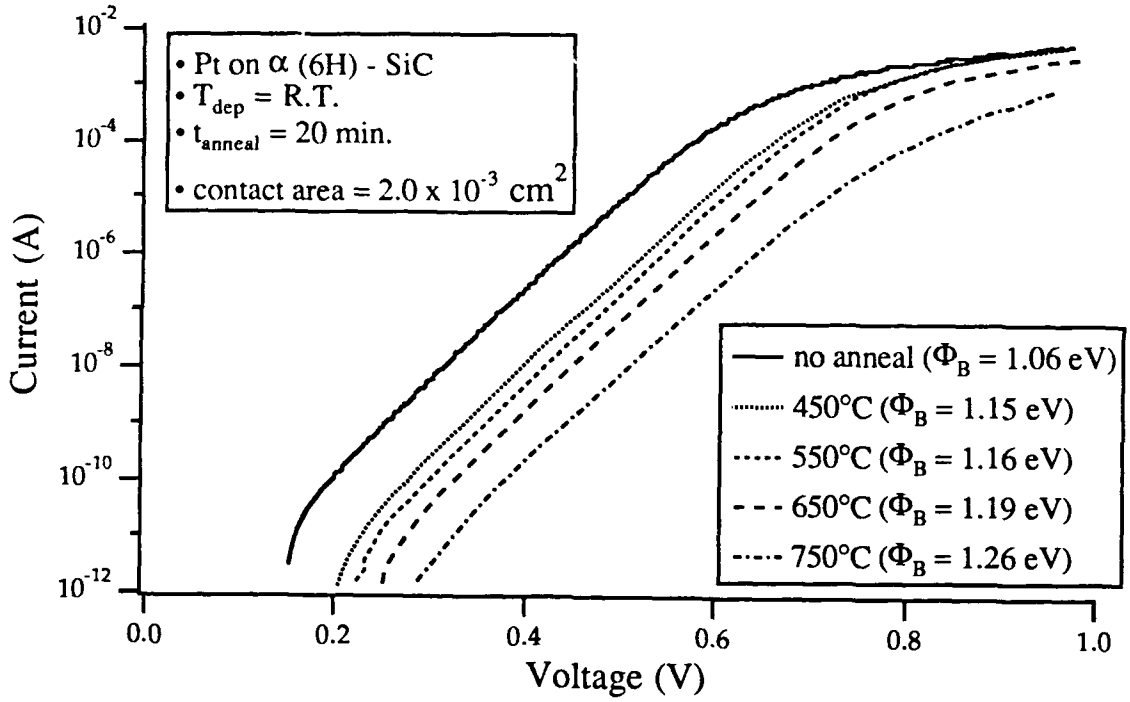

Figure 2. Log I vs. V of Pt/SiC through annealing series.

Figure 3. High resolution TEM micrograph of the interface between Pt and SiC.

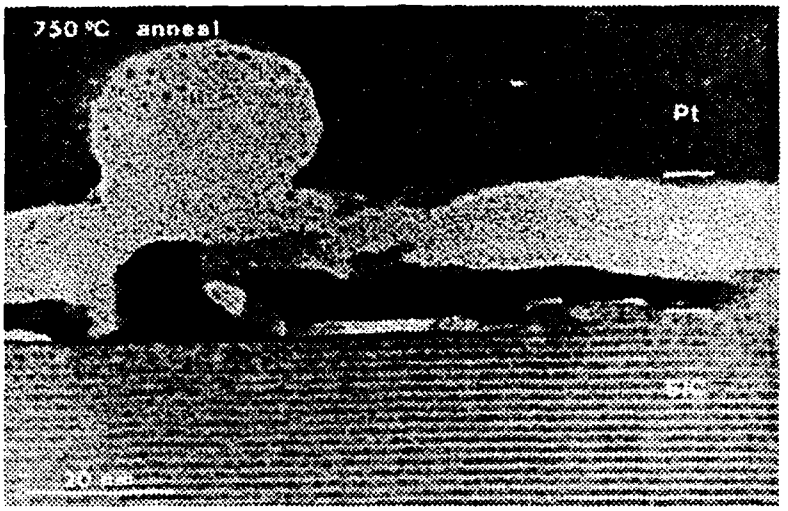

Figure 4. High resolution TEM micrograph of the Pt/SiC interface after annealing at 750°C for 20 min.

Hf Contacts. As for the Ti contacts, the Hf contacts were analyzed before and after annealing at 700°C for up to 1 hr. In all cases the contacts were rectifying with low ideality factors. The as-deposited contacts, which had a SBH of 0.97 eV, produced typical leakage currents of 2.5×10^{-7} A/cm^2 at –10 V. Annealing at 700°C for 20 minutes resulted in a reduction of the leakage to 4.0×10^{-8} A/cm^2. However, upon further annealing, the leakage currents increased.

Concomitant with the observable variation in the reverse characteristics with annealing time, the calculated SBH was found to vary. The 0.97 eV SBH for the unannealed contacts increased to 1.01 eV after the 20 min. anneal and then successively decreased to 0.93 eV and 0.86 eV for the 40 min. and 60 min. anneals, respectively. Qualitatively, the leakage current appears to vary inversely with the height of the barrier, as would be expected.

Although Hf has a smaller lattice mismatch with the (0001) basal plane of SiC than Ti, the as-deposited Hf film is polycrystalline. On the other hand, Hf has a larger lattice parameter than SiC; whereas Ti has a smaller one. Apparently it is more difficult to compress the Hf layer than it is to stretch the Ti layer. After annealing at 700°C there appears to be no formation of new phases.

Co Contacts. Cobalt has the highest SBH of the as-deposited contacts. SBH's of 1.14 eV and 1.16 eV were calculated from I–V and C–V measurements, respectively. As expected from the high barrier height, the leakage current was low, typically 2.5×10^{-8} A/cm^2 at –10 V (Fig. 5).

Because annealed Ni is used as an ohmic contact to n-type SiC and the chemical reactions between Ni and SiC and Co and SiC are similar [5, 6], the Co contacts were annealed for the purpose of creating ohmic contacts. Annealing for 20 minutes at 800°C in UHV did not produce ohmic contacts, but instead resulted in leaky diodes. The contacts did become ohmic

after rapid thermal annealing at 1000°C in an Ar or N_2 ambient. Figure 6 shows that the contacts became ohmic after annealing for a total of 2 min. but became much more resistive after annealing for 3 min. The characteristics were not investigated for annealing times less than 1 minute.

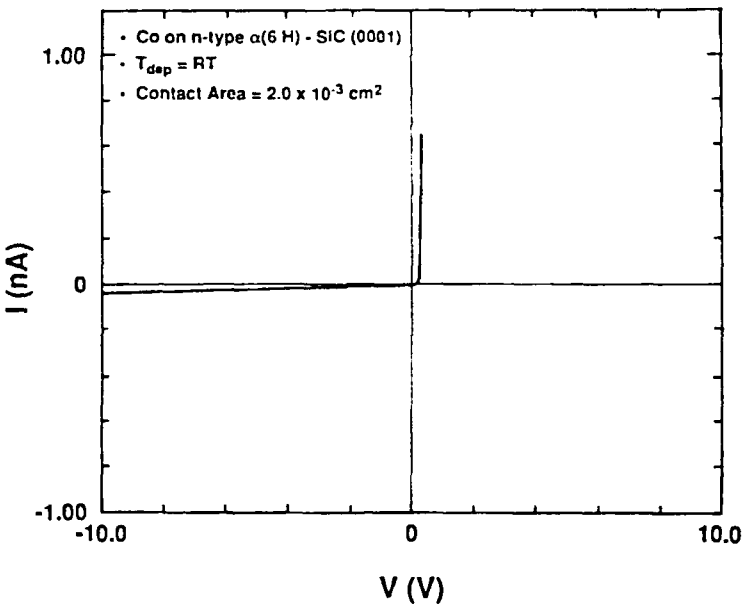

Figure 5. Current–voltage measurement of as-deposited Co on 6H-SiC. The contact structure consisted of a large area backside contact and a circular frontside contact (area 2.0×10^{-3} cm^2).

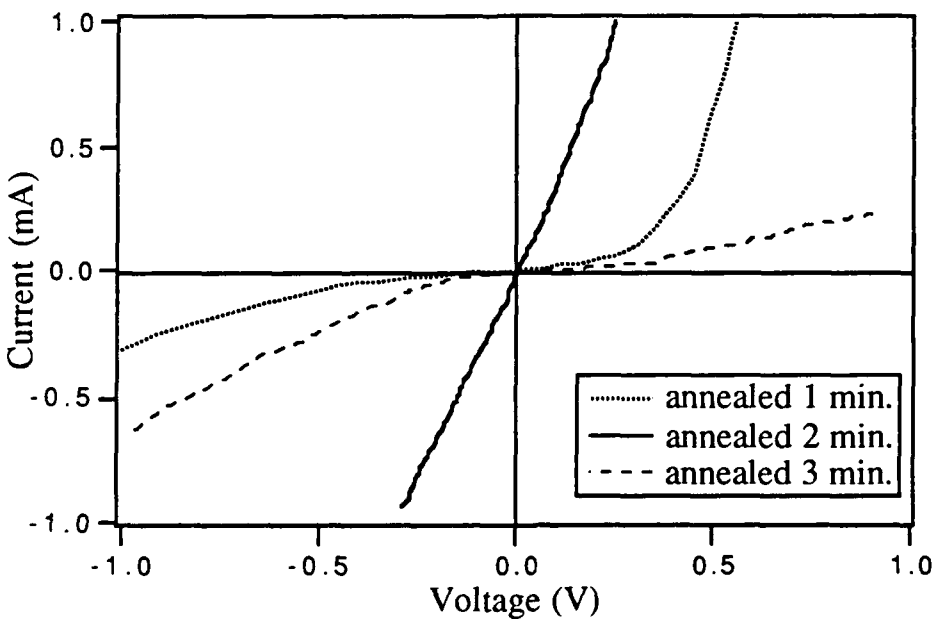

Figure 6. Current-voltage measurements of Co/SiC annealed for 1 min., 2 min., and 3 min. at 1000°C in an Ar ambient.

To measure the specific contact resistance Co was deposited onto SiC through a mask designed with TLM patterns. In this case both the substrate and epitaxial SiC had a carrier concentration of 3×10^{18} cm^{-3}. The specific contact resistance was 2×10^{-2} Ω cm^2. The high contact resistance may be due to the fact that the current was not confined to a low resistivity layer beneath the contact pads. It may be worthwhile to experiment with various annealing times, higher doped surface layers, and mesas to confine the current.

Initial results from HRTEM observation indicates that the as-deposited Co film is polycrystalline. However the film has a partial epitaxial relationship to the SiC substrate, with $(0002)_{Co}$ falling in the range of $\pm 5°$ along $(0006)_{SiC}$.

D. Discussion

Although each of the metal/SiC systems has its own characteristics, comparison of their properties reveals important information about the inherent properties of SiC contacts in general. The Schottky barrier height is a critical and quantitative parameter which determines the properties of a metal/semiconductor contact and, therefore, serves as a valuable comparison.

In the ideal case the SBH is defined by the Schottky-Mott limit, or the difference between the metal workfunction and the electron affinity of the semiconductor (for an n-type semiconductor). Table I shows the theoretical SBH's calculated form the workfunctions along with the SBH's calculated from I-V and C-V measurements.

Table I. Schottky barrier heights of metals on n-type 6H-SiC calculated from theory (Φ_B^{th}), current-voltage measurements (Φ_B^{I-V}), and capacitance-voltage measurements (Φ_B^{C-V}).

Metal	Φ_B^{th} (eV)	Φ_B^{I-V} (eV)	Φ_B^{C-V} (eV)
Hf	0.52	0.97	---
Ti	0.95	0.85	0.88
Co	1.62	1.14	1.16
Pt	2.27	1.06	1.02

Due to the wide range of metal workfunctions, the predicted SBH's range from 0.52 eV for Hf/SiC to 2.27 eV for Pt/SiC. However, the values calculated from I–V and C–V measurements only vary by a few tenths of an electron-volt. Figure 7 shows the theoretical barrier heights and the barrier heights calculated from I-V measurements both plotted vs. metal workfunction.

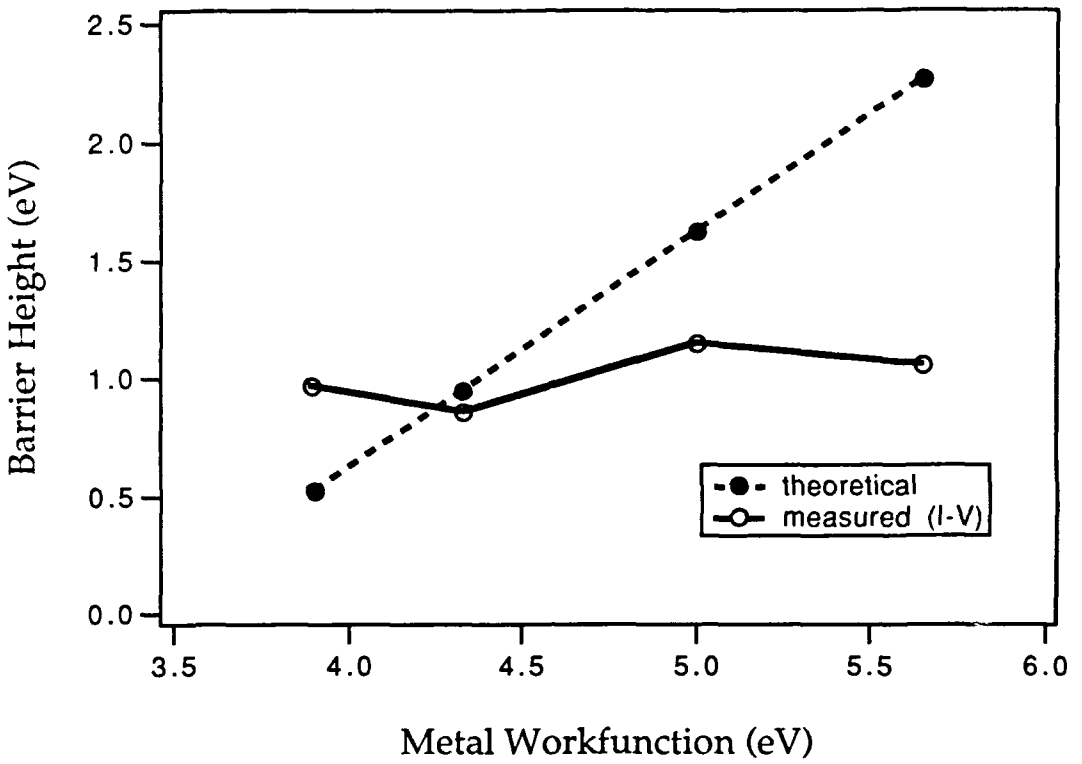

Figure 7. Theoretical and measured barrier heights of Hf, Ti, Co, and Pt on SiC plotted vs. metal workfunction. The values were taken from Table I.

Although in the ideal case the barrier height varies linearly with the workfunction of the metal, the actual barrier heights in this case appear to be quite independent of the workfunction. This independence has many implications for the SiC device engineer because controlling the contacts properties becomes more difficult.

The narrow range of calculated barrier heights is attributed to Fermi level pinning. This means that at the semiconductor surface the Fermi level is pinned at a fixed position relative to the conduction and valence bands due to surface or interface states. These surface or interface states accommodate charge transferred from the metal, which in the ideal case would be accommodated in the depletion region of the semiconductor, resulting in a change in band bending and hence a change in barrier height. J. Pelletier *et al.* [7] have reported Fermi level pinning in 6H-SiC attributed to intrinsic surface states, suggesting little dependence of barrier height on the workfunction of the metal. In addition, L. J. Brillson [8] predicts the pinning rate to be higher for more covalently bonded materials.

The next logical question would be whether there is any way to reduce these surface states or if there is any way of getting around this problem. The result that Ti, which grew epitaxially, had the closest barrier height to its predicted value may indicate that interface states are less between materials which have an epitaxial relationship. To further test this hypothesis,

a Ti-Hf alloy which should be closely lattice-matched to SiC was deposited. Since Ti and Hf have complete solid solubility, the barrier height should be somewhere in between 0.52 eV and 0.95 eV, the values which are predicted for pure Hf and pure Ti, respectively. In fact, the contacts were leaky, a result which is expected for a moderately low SBH. The SBH could not be calculated in this case. To determine how much effect epitaxial growth has on reducing interface states, an epitaxial film with a large workfunction should be deposited, and the resulting SBH should be calculated.

Because it may be difficult to grow epitaxial films with the desired properties, interlayers may prove to be a valuable solution to this problem. Thin layers (~10 Å) of semiconductors have been used to increase or decrease the SBH of metals on GaAs [9–13]. The basic idea is that with the appropriate band lineup, a semiconductor with a larger bandgap will result in a large SBH, while one with a smaller bandgap will result in a small SBH. This idea may also extend well to SiC. Because the SBH is pinned at a relatively high value (~1.0 eV), creating a small SBH is an important goal if interlayers are to be used. The smaller the SBH, the lower the contact resistance of an ohmic contact. Therefore, future plans involve the use of interlayers to reduce the SBH of metals to 6H-SiC.

E. Conclusions

Ti, Pt, Hf, and Co as-deposited at room temperature onto n-type 6H-SiC were all rectifying contacts with low ideality factors ($n < 1.1$) and low leakage currents. In addition, the Schottky barrier heights calculated from I–V and C–V measurements were all within two tenths of an electron volt of 1.0 eV. The narrow range of calculated barrier heights indicates that the Fermi level is pinned at the semiconductor surface. In order to have better control over the contact properties it will be important to overcome the problem of pinning, perhaps by use of interlayers.

F. Future Research Plans and Goals

Calcium, which has a very low workfunction, completes the original list of selected metal contacts. In the ideal case one would predict a negative Schottky barrier and hence an ohmic contact. After depositing a Ca layer, an Au layer will be deposited on top to prevent oxidation of the contact. Electrical measurements will then be taken, yielding an important, additional data point.

Very thin layers of n-type (P-doped) Si will be deposited on the SiC surface prior to deposition of the metal contact. The purpose of the Si interlayer will be to reduce the barrier at the metal contact and hence promote ohmic behavior. X-ray photoelectron spectroscopy will be used to examine the chemistry and to determine the amount of band bending at the Si/SiC interface. Electrical measurements will be taken of the metal/Si/SiC contacts.

G. References

1. Berger, H. H., Solid State Elect. **15**(2), 145 (1972).
2. Porter, L. M., *et al.*, Mat. Res. Soc. Symp. **282**, 471 (1993), (in press).
3. Spellman, L. M., *et al.*, Mat. Res. Soc. Symp. Proc. **221**, 99 (1991).
4. Papanicolaou, N. A., A. Christou, and M. L. Gipe, J. Appl. Phys. **65**(9), 3526 (1989).
5. Nathan, M. and J. S. Ahearn, J. Appl. Phys. **70**(2), 811 (1991).
6. Chou, T. C., A. Joshi, and J. Wadsworth, J. Mater. Res. **6**(4) 796 (1991).
7. Pelletier, J., D. Gervais, and C. Pomot, J. Appl. Phys. **55**(4) 994 (1984).
8. Brillson, L. J., Phys. Rev. B **18**(6), 2431 (1978).
9. Chambers, S. A. and T. J. Irwin, Phys. Rev. B. **38**(11), 7484 (1988).
10. Chambers, S. A., V. A. Loebs, and D. H. Doyle, J. Vac. Sci. & Tech. B **8**(4), 985 (1990).
11. Chambers, S. A. and V. S. Sundaram, Appl. Phys. Lett. **57**(22), 2342 (1990).
12. Chambers, S. A. and V. A. Loebs, J. Vac. Sci. & Tech. A **8**(3), 2074 (1990).
13. Chambers, S. A. and V. A. Loebs, J. Vac. Sci. & Tech. B **8**(4), 724 (1990).

IV. Electronic Properties of Metal-SiC and AlN-SiC Surfaces and Interfaces

A. Introduction

SiC has characteristics that make it a good candidate for high power and high temperature device use. We have initiated investigations of 6H n-type SiC as a rectifying contact. To this end, we will employ uv-photoemission to measure the Schottky Barrier height (SBH) as a function of metal type and thickness deposited on the SiC substrates. In the Schottky-Mott model of the electronic properties of the metal-semiconductor interface, the barrier depends only on the work function of the metal and the electron affinity of the semiconductor. However, for most practical situations there will be a dependence on electronic states at the interface. These states result in a dipole at the interface and will substantially affect the Schottky barrier.

Independent of model, the SBH for a n-type semiconductor is the difference between the metal Fermi level and the conduction band minimum, while for a p-type semiconductor the SBH is the difference between the Fermi level of the metal and the valance band edge. The SBH can be deduced from Ultraviolet Photoemission Spectroscopy (UPS) measurements. The measurements involve directing 21.2 eV light (the HeI resonance line) to the surface of the sample and counting the photo excited electrons as a function of electron kinetic energy. The measurement gives a profile of the valance band(VB) since the light promotes electrons from the VB to the conduction band (CB) by shifting the energy by 21.2 eV. From the spectra the VB edge can be determined from the onset of electron emission. A thin metal layer can then be deposited on the semiconductor and we can determine the Fermi level. Thus the SBH for a p-type semiconductor can be measured directly. For an n-type semiconductor the SBH is given by the bandgap energy minus the measured p-type barrier.

Before deposition of metals on the substrate, it is necessary to insure that a clean surface without defects or graphitization is obtained. This will be verified by examining the surface stoichiometry as a function of annealing temperature. The tools used will be Low Energy Electron Diffraction (LEED) and Auger Electron Spectroscopy (AES). Cleaning methods investigated will include UHV annealing, *in situ* state-of-the-art remote plasma cleaning, and *ex situ* as chemical techniques.

A new area of research that has been initiated in this program is the study of the electronic properties of AlN surfaces grown on SiC substrates. AlN is a wide bandgap material (6.3 eV) with potential semiconductor applications. Bulk samples grown to date are highly insulating making electronic property measurements impossible. Recent developments of new growth methods have shown that high quality AlN can be grown epitaxially on SiC substrates. We show for the first time in this report that these thin films can be studied by photoemission spectroscopy. Initial spectra of the AlN seem to indicate a Negative Electron Affinity (NEA).

In this report, initial work is reported on bare SiC substrates and on AlN that was grown on a SiC wafer. The AlN-SiC sample was grown by MBE by Cheng Wang, working with R. F. Davis.

B. Procedure and Results

The SiC samples used are 6H n-type wafers supplied by Cree Research. The samples have doping concentrations of ~10^{15} to 10^{16} /cm^3. All work done has been on the Si-terminated (0001) face. The *ex situ* cleaning technique used an HF spin etch with a solution of HF:H_2O:ethanol at 1:1:10. This technique was developed for the cleaning of Si wafers. The *ex situ* clean was followed by annealing in an ultra high vacuum environment with a base pressure of 10^{-9} Torr. As loaded, the sample exhibited a 1×1 LEED pattern. LEED patterns were obtained after anneals of 700, 1000, and 1200 °C. The patterns in all cases were 1×1. Auger Electron Spectroscopy (AES) was done after the 1200°C anneal. The spectra were noisy when we used the Perkin-Elmer 11-500 AES system with a SRS Lock-in amplifier. The projection is that our new system, a Perkin-Elmer 3017 package will provide much better resolution. However, our current Auger spectra show an average C/Si ratio of 0.331 which compares favorably to the results, at the same temperature, of S. Nakanishi, *et al.*[1]. An ideal starting surface would exhibit a ratio of 1.

Preliminary UPS data have been obtained in a separate system, with the same base pressure. The UPS results are shown in Fig. 1. The as loaded UPS measurements showed features attributed to oxygen on the surface. After UHV annealing to greater than 700°C the spectra show a substantial change with a reduction in the features due to oxygen. However, other features which represent the electronic structure of the SiC also disappear. These spectral changes are then attributed to a highly defective surface. The spectra clearly showed that the cleaning process had to be refined.

The UPS results obtained from AlN -SiC are shown in Fig. 2. The spectra have been normalized to the Fermi energy. The spectra show weak emission from the valence band maximum which increases nearly monotonicaly for decreasing electron kinetic energy. Typically UPS spectra are obtained with the sample grounded to the same potential as the electron analyzer. If the work function of the electron analyzer is larger than that of the sample then the low energy photoemitted electrons are not detected. However, a small bias applied between the sample and the analyzer can add enough energy to the photoemitted electrons to overcome the analyzer work function. Since metal work functions are ~4–5 eV then a bias of < 2V is usually sufficient. The application of a bias can easily be accomplished by inserting a battery and a potentiometer between the sample and its connection to ground.

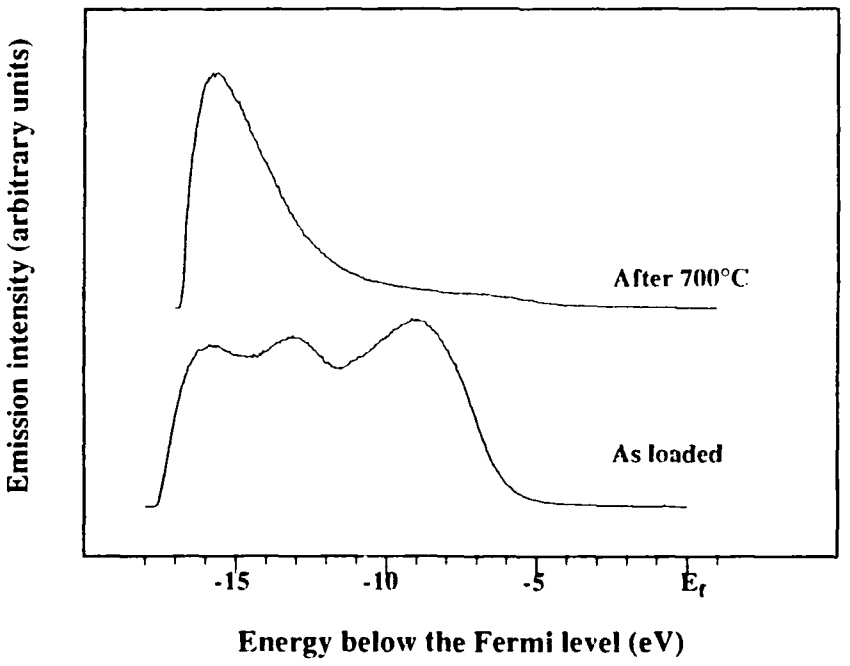

Figure 1. The UPS spectra of SiC surfaces (a) after chemical cleaning and (b) after annealing to > 700°C. The spectra were excited with 21.2 eV HeI light, and the photoemitted electrons were collected at normal emission.

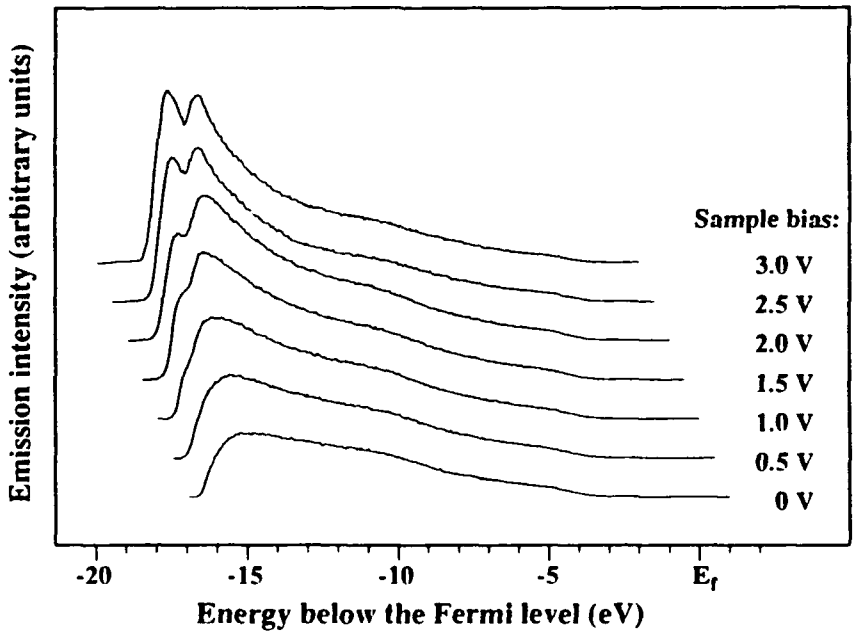

Figure 2. The UPS spectra of a AlN - SiC sample as a function of bias on the sample. Photoemission was obtained as in Fig. 1. As the sample bias is increased low energy electrons are able to overcome the work function of the electron analyzer. The peak that appears with increased bias is attributed to a negative electron affinity of the AlN surface.

Also shown in Fig. 2 is a series of spectra obtained at sample bias' ranging up to 2V. We note that the spectral features near the valence band maximum are not changed with sample bias. In contrast, the spectral features at the lowest kinetic energy are substantially changed. As the bias is increased to 1.5V a shoulder appears at the lowest kinetic energy. As the bias voltage is increased, this feature continues to increase in strength to the point where it is the strongest feature in the spectra. Features similar to this have recently been observed on diamond surfaces and have been attributed to the presence of a negative electron affinity. [3]

C. Discussion

With regards to the SiC surfaces, the presence of oxygen at various levels was detected with all of the cleaning methods used. In addition, the lack of spectral features on the cleaned SiC surface indicated that the surface contained substantial defects. This was reflected in the AES results which indicated that while the presence of oxygen on the SiC surface might not be critical for growth of refractory metals such as Ti, it could strongly affect the electronic properties. For example, L. Spellman, using the same cleaning method, was able to grow Ti epitaxially on SiC. [2] The effects of the defects or impurities on the electronic states and Schottky barrier has not yet been established, but for most semiconductor 10^{12} interface states per cm^2 is usually enough to pin the Fermi energy. Current oxygen impurity and surface defects due to non stoichiometry are 10 to 1000 times greater than these levels.

The new Auger system is connected by a transfer line to the UPS chamber. The plasma and MBE chambers are also connected to this line so that all the measurements can be made without leaving the UHV environment. Recently two new chambers were added to the transfer line. These are an Auger/XPS system and a Gas Exposure/Growth chamber. With these facilities it should be possible to control and characterize the surface properties to an extent not previously achievable.

The AlN–SiC results hold potential for a whole new series of device structures based on cold cathode electron emitters. The relatively sharp peak that is observed at the low energy end of the UPS spectra is similar to results obtained from diamond surfaces which exhibit a NEA. In diamond, this feature has been attributed to electrons which have been quasi thermalized to the conduction band minimum. The only way that electrons from the conduction band minimum can escape is if the vacuum level is less than the conduction band minimum (ie. negative electron affinity). Thus, electrons near the surface can escape.

For highly insulating materials, after few electrons are emitted the electron emission will be quenched due to charging. The fact that the electron emission is not quenched in these AlN–SiC samples is an important result indicating that the surface electrons are replenished from the SiC substrate.

For diamond it was found that the NEA was highly dependent on the surface processing. We would anticipate the same for AlN. Because the samples used in this study were transferred in air, they certainly had some oxide present. In addition, it is well known that H bonds to the surface. The role of oxygen, hydrogen or other surface impurities will be the subject of future studies.

D. Conclusions

As indicated here more work is needed on the cleaning of the SiC surface prior to metal deposition. The goal will be to obtain stoichiometric surfaces with defect and impurity concentrations less than $10^{12}cm^{-2}$. With the new equipment developments it should be possible to control and characterize the surface properties to an extent not previously achievable.

This report shows the first UPS measurements of the electronic states of AlN. The results indicate that the AlN-SiC structures exhibit a negative electron affinity. In addition, the emission is apparently not limited by the wide bandgap and typical insulating character of AlN.

E. Future Plans

The goal of the work is to develop rectifying contacts for use as diodes. To this end, we will attempt to ensure that we have a clean surface for deposition of metals. We will use LEED and AES to examine surface stoichiometry as a function of annealing temperature in an effort to maximize oxygen removal while minimizing graphitization of the sample. Once the cleaning is adequate for epitaxial growth we will deposit, epitaxially, metals starting with Ti and leading to Hf, Ni, and Zr. Ultraviolet Photoemission Spectroscopy (UPS) will be used to determine the Schottky Barrier height. We will determine the dependence of the Schottky Barrier height on the type and thickness of deposited metals. Chemical cleaning is being used at present and plasma cleaning will be assessed. Future plans involve the addition of *in situ* Raman to the connected systems. The two new systems mentioned in the discussion section might also be incorporated into the research. These will allow further characterization of the contacts.

The work on AlN-SiC has shown the potential for a new series of electronic devices based on electron emission from negative electron affinity surfaces. Future work will explore the effects of oxygen, hydrogen and other defects and impurities on the electron affinity of these complex structures.

F. References

1. S. Nakanishi, *et. al.*, Applied Surface Sci. **41/42,** 45 (1989).
2. L.M. Spellman, *et. al.*, Mat. Res. Symp. Proc. Vol. 221 (1991).
3. J. van der Weide and R.J. Nemanich, Appl. Phys. Lett. **62**, 1878 (1993).

V. Determination of the Diffusivity of Si, C, Al and N at the Interface of the SiC-AlN Diffusion Couple

A. Introduction

Silicon carbide has long been of interest because of its superior structural, thermal and electrical properties. High temperature and/or erosion- and corrosion-resistant wear parts, as well as, optoelectronic and microelectronic semiconductor devices are representative applications. Control of the physical and chemical properties of SiC via microstructural changes achieved by using different processing routes has been extensively studied for many years. The microstructural variables most frequently changed include the amount and the morphology of the various polytypes in the processed material, intentionally introduced second and additional phases and additions of sintering aids which may or may not form a grain boundary phase. The processing temperature, impurity content, and sintering (or annealing) atmosphere affect the resultant microstructure. However, the primary material remains SiC. Another approach to property engineering involves the alloying of SiC with other ceramic compounds to alter, e. g., the band gap. This approach has also been of interest for several years.

One compound which has been reportedly alloyed with α(6H)-SiC (a_0 = 3.08Å) is AlN (a_0 = 3.11Å) due to the similarities in the atomic and covalent radii and the crystal structures. Diverse processing routes have been employed to achieve partial or complete solid solutions from these two compounds including reactive sintering or hot pressing of powder mixtures and thin film deposition from the vapor phase [2–5,8,16–20,22,23]. There exists, however, a difference in opinion among investigators regarding the occurrence and the extent of solid solutions in the SiC-AlN system at temperatures < 2100°C.

Schneider [1] concluded that the formation of $(AlN)_x(SiC)_{1-x}$ solid solutions of were not favorable within the temperature range of his study of the AlN-Al_4C_3-SiC-Si_3N_4 system. He found two phase mixtures rather than $(AlN)_x(SiC)_{1-x}$ solid solutions when equal molar ratios of either SiC and AlN or Si_3N_4 and Al_4C_3 were hot pressed at 1760°C–1860°C for 45 and 30 minutes, respectively. Subsequently, Zangvil and Ruh [4] prepared sintered samples of varying compositions by cold pressing powdered mixtures of SiC and 10–50 wt % AlN and subsequently hot-pressing them in vacuum. Microstructures of the samples hot-pressed within the range 1850–1950°C revealed partially sintered AlN grains and β-SiC grains of unusually large size. Ruh [2,19,26] using dry mixtures of SiC and AlN powders, hot-pressed in vacuum under the conditions of 35MPa and 1700–2300°C obtained no SiC-AlN solid solution for temperatures ≤ 2100°C and concentrations of ≈35 to 100 mol % AlN. In contrast, Rafaniello [8] reported solid solutions as indicated by X-ray diffraction in samples only hot-pressed at 1950°C–2300°C and 70 MPa for ≈3 h in Ar. However, he subsequently showed [3] using a

more careful analysis of his X-ray diffraction data that the broadening of the SiC-AlN peak was caused by the existence of a two-phase region and not the 2H solid solution previously reported [8]. The initial confusion was caused by the closeness (≈1%) in the lattice parameters of SiC and AlN. This was supported by optical microscopy of multiphase assemblages in the sintered samples for temperatures as high as 2300°C. Rafaniello [3] also revealed strong evidence of a miscibility gap by the precipitation of SiC-rich phase from 75 wt % AlN solid solution and precipitation of an AlN-rich phase from a 47 wt % AlN alloy, when hot-pressed samples were annealed at 1700°C for 90h. Modulated structures were found by Kuo [5] for samples with equimolar compositions below ≈ 1900°C and in samples containing 25 mol % SiC - 5 mol % AlN annealed at 1700°C for 170 h. Likewise, Chen [22] hot-pressed a mixture of β-SiC and AlN powders in nitrogen at ≈2300°C for 20 min to 3.5 h. Samples were then annealed in nitrogen (1 atm) over a range of temperatures between 1600°C–2000°C for up to 1145 h. Modulated structure development in samples of equimolar composition annealed at 2000°C and below indicated that 2000°C is below the coherent spinodal which would give further evidence of a miscibility gap as reported by Rafaniello [3], Kuo [5] and Sugahara [6].

Common to all the investigations described above was the use of AlN and β-SiC powders supplied by Herman Starck and the high concentrations of impurities contained in these materials. The concentration of oxygen and boron in starting powders [2–5,8,18–20,22,23] is significant. Xu and Zangvil [18] found small Al_2O_3 inclusions embedded in 2H grains of SiC-AlN samples uniaxially prepressed at room temperature to 35 MPa and subsequently hot-pressed at 2150°C at a pressure of 40 MPa in a flowing nitrogen atmosphere (1 atm.). The oxygen needed for the formation of the Al_2O_3 inclusions was beyond the 2% content reported in the analysis of the as-received AlN and, therefore, was probably introduced during processing. This is of considerable importance since Tajima [9] found that in the temperature range of 1800°C–2000°C the solid solubility of aluminum in SiC may be influenced by impurities and by the heating atmosphere; since, the defect structure of SiC would be affected by these factors. He also found conclusive evidence that aluminum atoms substitute for silicon in SiC. Furthermore, Zangvil [4] suggested that aluminum and nitrogen move as well as silicon and carbon as diffusion couples to ensure a local charge balance during mass transport. This process would be strongly impurity dependent and therefore control the solid solution formation. Oden [20] attempted to deal with the issue of impurities by preparing Al_4C_3 and SiC and comparing these with Hermann Starck- SiC and Cerac- AlN. The impurities of the latter materials were reported, however, those contained in Oden's materials were not. It was suggested by Oscroftt [21] that the oxygen content present in both materials was very high. Furthermore, the highly reducing nature of the graphite hot-pressing die may be the controlling factor in the oxygen content for both pure and impure materials [21]. Further evidence of the effects of oxygen was presented in a later study by Kuo [27] who found the existence of an

extensive, if incomplete, solid solution between AlN and Al_2OC at temperatures in excess of 1900°C. Below about 1800°C, the 2H solid solution was unstable and decomposed into two solid solutions of 2H crystal type as shown by the presence of extremely fine precipitates developed during cooling. The kinetics of solid solution formation were relatively rapid when compared with the SiC-AlN system, assuming such solutions actually occur in this latter system. This is of considerable importance when considering the high oxygen content in starting AlN materials. It should also be noted that two different phase diagrams have been presented for the SiC–AlN system Zangvil and Ruh [26] and Patience [30]. The most widely accepted was proposed by Zangvil and Ruh [26]. It is based on data obtained from numerous sintering experiments [2-4,8,19].

In contrast to the studies described above are reports of the formation of solid solutions between SiC and AlN at relatively low processing temperatures (i.e. within the proposed miscibility gap region). Cutler [7] formed solid solutions between SiC and AlN from 2 mol % to 100 mol % AlN with a single wurtzite type phase, as determined by X-ray diffraction. This was accomplished by the carbothermal reduction of fine amorphous silica ('cabosil'), precipitated aluminum hydroxide, and a carbon source of starch/sugar in a nitrogen atmosphere at 1400°C–1600°C. In subsequent work, by Rafaniello [8], intimate mixtures of SiO_2, Al_2O_3 and C were reacted at 1650°C for 4 h in flowing N_2. Solid solutions over the entire composition range were reported.

Processing conditions and impurities were shown to be a factors affecting the solid solution formation by Czekj [24]. He prepared solid solutions of 2H-$(AlN)_x(SiC)_{1-x}$ from rapid pyrolysis ("hot drop") of organometallics at temperatures < 1600°C. In contrast, slow pyrolysis of mixtures produced compositions rich in 2H-AlN and 3C-SiC at 1600°C which were later transformed to 2H-$(AlN)_x(SiC)_{1-x}$ solid solutions after heating to 2000°C. Jenkins, *et al.* [16] reported the growth of solid solutions of $(AlN)_x(SiC)_{1-x}$ by MOCVD over the entire composition range from 20 % to 90 % AlN in the temperature range of 1200°C–1250°C, as measured by Auger spectroscopy. Kern [17] reported growth of a high purity $(AlN)_{0.3}(SiC)_{0.7}$ solid solution at 1050°C by plasma-assisted gas source molecular beam epitaxy.

Theoretical calculations of the immiscibility region in the $(AlN)_x(SiC)_{1-x}$ system were conducted by Sukhanek [28] using the dielectric theory of A^NB^{8-N} semiconductors. The theory relates changes in the band structure to the enthalpy of formation in semiconductors. He concluded that the formation of a continuous series of solid solutions of silicon carbide with aluminum nitride were possible above 1000°K. This was shown by Shimada [10] who hot pressed mixtures of SiC, Si_3N_4, AlN and Al_3C_4 powders at 1300°C - 1900°C and 3.0 GPa for 1 h and reported the formation of solid solutions by X-ray diffraction. Tsukuma [11] also sintered mixtures of Si_3N_4 and Al_4C_3 in a gas autoclave at 1800°C and 10 MPa in argon. Solid solutions rich in AlN were produced. However, solutions in the SiC-rich region could not be

formed under the same conditions. Zangvil [12] suggested that this phase was a solid solution of $(AlN)_x(SiC)_{1-x}$ based on lattice parameters; however he also noted that he found no solid solution at 1900°C in vacuum and that Schneider [1] did not form solid solutions at 1860°C. It is interesting to note the short processing time < 1 h. Tsukuma's [11] findings are consistent with the proposed kinetics and reaction path described by Rafaevich [29] and Mitomo [15].

Rafaevich [29] used conditions similar to Zangvil [4] to determine the kinetics of the reaction between Si_3N_4 and Al_3C_4. The purpose of his work was to determine the formation mechanism of the $(AlN)_x(SiC)_{1-x}$ solid solutions during sintering. Diffraction patterns after sintering for 0.5 h at 1950°C in 1 atm of nitrogen indicated that SiC had not completely formed and that Si_3N_4 was still present. Sintering for 1 h at 1950°C indicated that Si_3N_4 had completely transformed into SiC; however, solid solutions of SiC-AlN had not completely formed. Sintering for 1.5 h at 1950°C showed a complete, homogeneous $(AlN)_x(SiC)_{1-x}$ solid solution. Reaction paths studied by Mitomo [15] were determined by the formation of a uniformly dispersed composite powder of β-SiC and 2H-AlN using an alkoxide-derived SiO_2-Al_2O_3 mixture. The total reaction was carried out at 1500°C and of the form:

$$2SiO_2 + Al_2O_3 + 9C + N_2 \rightarrow 2SiC + 2AlN + 7CO$$

The large amounts of carbon (3.7 time the normal amount) were needed to complete the reaction. Reactions observed at 1500°C were

$$2SiO_2 + Al_2O_3 + 10.5C \rightarrow 1.5SiC + 0.5Al_4SiC_4 + 7CO$$

$$1.5SiC + 0.5Al_4SiC_4 + N_2 \leftrightarrow 2SiC + 2AlN + 1.5C$$

Large weight loss after the reaction was attributed to the evaporation of SiO_2 as SiO. Mitomo [15] suggested that SiO_2 and Al_2O_3 reacted in sequence with carbon. This is of substantial use in the evaluation of the reported attempts to form solid solutions which have been previously published. The indication is that the formation of $(AlN)_x(SiC)_{1-x}$ solid solutions using SiO_2 and Al_2O_3 in a N_2 atmosphere is not favorable for short sintering times due to the complex reaction scheme.

Zangvil [4] has approximated the diffusion coefficients between SiC and AlN to be 10^{-12} $cm^2 \cdot s^{-1}$. The corresponding activation energy and pre-exponential term were estimated to be as high as 900 kJ·mol, and 10^{-8} $cm^2 \cdot s^{-1}$, respectively. Three reasons for these values were suggested by Zangvil [4]: (1) SiC penetration among AlN grains in the early stages of sintering (2) material transport by gaseous species, and (3) lattice diffusion of coupled SiC and AlN pairs.

The purpose of this investigation has been to determine the extent of solid solution formation within the temperature range of 1700°C–1850°C and to determine the diffusion

coefficients and the corresponding activation energies for the four elements Si, C, Al and N within this solution. It is clear that the atomic behavior and the extent of phase formation at relatively low temperatures for thin film deposition cannot be discerned from the research conducted previously. Likewise, the diffusivities of these species have not been studied for epitaxially deposited AlN on single crystal SiC.

B. Experimental Procedures

Sample Preparation. Samples were prepared in a modified Perkin-Elmer 430 molecular beam epitaxy (MBE) system. Aluminum (99.999%) was evaporated from a standard effusion cell. Activated nitrogen was achieved using an MBE compatible, electron cyclotron resonance plasma source. Single crystal AlN with very few planar defects was epitaxially deposited on vicinal α(6H)-SiC [0001] wafers manufactured by Cree Research, Inc. and cut off axis 3°–4° toward [11$\bar{2}$0]. Growth conditions for the films are presented in Table I.

Table I. Growth Conditions for the 2H AlN films on α(6H)-SiC(0001) substrates

Nitrogen pressure	2×10^{-4} Torr
Nitrogen flow rate	4–5 sccm
ECR microwave power	50 W
Substrate temperature	650°C
Growth rate	≈ 0.1μm/hr
Total growth time	7–8 hrs.

Transmission electron microscopy (TEM) (Hitachi H-800) photos have been taken of the 2H-AlN (wurtzite) film on the α(6H)-SiC substrate before annealing and show a smooth and abrupt interface. Several different precautions were taken in order to prevent contamination of the samples and to minimize the loss of volatile components principally aluminum, and nitrogen. The samples were placed in a high density pyrolitic graphite crucible shown schematically in Fig. 1. The inside of the crucible was previously coated with SiC by heating a mixture of Si and β-SiC inside the holder to 2000°C. The diffusion samples were placed inside this holder with the α(6H)-SiC(0001) face against the SiC coating. Bulk AlN squares were then placed on top of the deposited AlN. The holder was then closed using a threaded lid and loaded into the furnace. The chamber was evacuated (2×10^{-6} torr) to prevent contamination during diffusion. N_2 gas (99.9995%), purified by a gettering furnace containing heated Cu chips (Centorr Furnace model 2B-2O) was then introduced into the chamber at a rate of

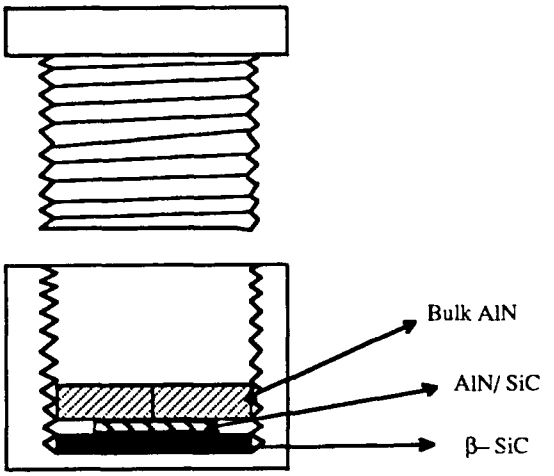

Figure 1. Schematic of a high density pyrolitic graphite crucible.

365 sccm. The chamber was brought to atmospheric pressure and a flowing N_2 environment maintained throughout each diffusion anneal. Diffusion temperatures were reached in ≈20 min (exact value for 1850° C). The samples were then removed for characterization. The N_2 gas, bulk AlN, and SiC coated crucible are not meant to aid in the diffusion. This was checked by a SiC-AlN standard which had not been annealed. The AlN as well as the SiC intensity in the standard were the same as AlN and SiC intensity outside of the diffused region. The samples were diffused for a temperature range of 1700°C to 1850°C for as wide a range of times as possible. A complete listing of temperatures and times are given in Table II.

Table II. Annealing conditions used to date for the AlN/SiC diffusion couples

Sample #	Temperature (°C)	Time (hrs)
32	1850	25
28	1850	21.5
21	1850	10
26	1800	30
31	1800	25
29	1800	20
27	1750	70
23	1750	50
18	1750	25
33	1700	70
19	1700	30

Characterization–Auger Spectroscopy. Scanning Auger microprobe (SAM) (JEOL JAMP-30) analysis was used to determine the concentration verses diffusion distance for all samples in Table II. Samples were tilted at a 60° angle in order to minimize charging effects. An argon ion sputtering unit attached to the SAM was used to sputter through the samples while data was being collected. Sputter rates were determined for the Ar ion beam in three different types of media namely, AlN, SiC and their solid solutions. This was accomplished by 5, 10 and 15 minute sputter rates on AlN and SiC then extrapolated for longer times in each medium. The depths were measured using a profilometer. The sputter rates for the solid solution region were determined by measuring the depth of different samples of different sputter times where the ion beam had sputtered through the entire diffused region and subtracting the sputter times for AlN and SiC. This rate was plotted and extrapolated for longer times. Knowing sputter rates for each material allowed for the conversion of sputter time to distance. Sputter rate standards also served as standards for the 100% intensity peaks for Al, N, Si, and C from which relative concentrations were obtained.

Characterization–Transmission Electron Microscopy. The samples was cut into 3 micron wide and 500 micron thick discs which were mechanically thinned to about 100 microns and dimpled at the SiC-AlN interface to a final thickness of 20 microns. Further thinning of the samples with an ion miller achieved an electron transparent area. An acceleration voltage of 6 kV for initial milling was used; it was decreased to 4 kV for the final milling. The milling angles of 15°, 12°, and 6° were used in sequence during the milling. TEM observations were subsequently conducted using Akashi EM-002B Ultra-High Resolution TEM at 200 kV. The TEM was conducted only on the longest runs to demonstrate microstructure.

C. Results

From Auger depth profiles it is apparent that diffusion has occurred and from the smoothness of the concentration verses distance profiles there is no indication of a two-phase region for samples annealed between 1700°C–1850°C. This indicates that complete solid solution formation over the entire composition range has been obtained. Using calculated sputter rates, values of concentration verses diffusion distance were determined. The Boltzmann-Matano diffusion equations were used to determine the diffusion coefficients for each element. It is possible that the α(6H)-SiC is transformed to the 2H-SiC polytype as a result of its initial contact with the AlN. If this is true, the calculated activation energy should be reduced by the amount of energy needed to transform the α(6H)-SiC to 2H-SiC. The solid solution subsequently occurs between the 2H-SiC and 2H-AlN via coupled diffusion in order to maintain local charge equilibrium. It should be noted that this is not the only means of forming the 2H solid solution. It is also possible that the diffusion of AlN into SiC causes the

transformation of SiC to the polytype 2H. In this case the reduction of the activation energy by the transformation energy may be incorrect.

In order to determine the diffusivities of the four components of the process the Boltzmann-Matano solution of the diffusivity, D, as a function of concentration, distance, and time (c, x, t) is being employed. At this writing, the Auger data is being carefully analyzed to ensure that diffusion has actually occurred between these two materials. The reason for this uncertainty is derived from the fact that in a parallel investigation of the apparent diffused region using electron energy loss (EELS) in cross-sectional TEM with a 15Å beam, the presence of Al and N as well as Si and C have not been observed in the SiC layer and the AlN film, respectively. Bright field TEM of the surface in cross section has revealed a stepped surface with very high steps. As such, it is important to make absolutely sure that the Auger electron beam is not detecting components from two different steps and thus giving an apparent diffusion profile rather than providing data of a real profile from the formation of solid solutions.

D. Future Research

Additional diffusion anneals will be conducted between 1750 and 2000°C using the same procedure described above. Special care will be used to ensure that a flat AlN surface is achieved after the diffusion experiments and prior to the Auger Depth profile studies. A quartz flat coupled with a He lamp will be used to check the flatness of the AlN surface. Light polishing with diamond paste will be used to produce the flat surface if it is not present after the diffusion anneals. Additional studies to be conducted in tandem with the diffusion runs include (1) the fabrication of solid solutions using MBE and the subsequent annealing at high temperatures to determine if either segregation of the AlN and SiC occurs or if the solid solution is maintained, thus proving that it is an equilibrium phase and (2) the additional use of EELS to determine if interdiffusion can be discerned at any temperature.

E. References

1. G. Schneider, L. J. Gauckler and G. Petzow, Material Science Monographs **6**, 399 (1980).
2. R. Ruh, A. Zangvil, J. Am. Ceram. Soc. **65** [5], 260 (1982).
3. W. Rafaniello, M. R. Plichta, A. V. Virkar, J. Am. Ceram. Soc. **66** [4], 272 (1983).
4. A. Zangvil, R. Ruh, J. Mat. Sci. and Eng. **71**, 159 (1985).
5. S. Kuo, A. V. Virkar, W. Rafaniello, J. Am. Ceram. Soc. **70** [6], C-125 (1987).
6. Y. Sugahara, K. Sugimoto, H. Takagi, K. Kuroda, C. Kato, J. Mat. Sci. Lett. **7**, 795 (1988).
7. I. B.Cutler, P. D. Miller, W. Rafaniello, H. K. Park, D. P. Thompson and K. H. Jack, Nature **275**, 434 (1978).
8. W. Rafaniello, K. Cho, A. V. Virkar, J. Mater. Sci. **16** [12], 3479 (1981).
9. Y. Tajima, W. D. Kingery, Am. Ceram. Soc. [2], C-27 (1982).

10. M. Shimada, K. Sasaki, M. Koizumi, Proc. of Inter. Sym. on Ceram. Components for Engines, (1983).
11. K. Tsukuma, M. Shimada, M. Koizumi, J. Mater. Sci. Lett. **1**, 9 (1982).
12. A. Zangvil, R. Ruh, J. Mater. Sci. Lett. **3**, 249 (1984).
13. K. A. Schwetz and A. Lipp, in *Am. Ceram. Soc.* 89th Annual meeting abstracts, The American Ceramic Society, Westerville, OH, p. 30, 1987.
14. R. A. Youngman, J. H. Harris, J. Am. Ceram. Soc., **73** [11], 3238-46 (1990).
15. M. Mitomo, M. Tsutsumi, Y. Kishi, J. Mat. Sci. Lett. **7**, 1151-1153 (1988) .
16. I. Jenkins, K. G. Irvine, M. G. Spencer, V. Dmitriev, N. Chen, J. Cry. Gro. **128** 375-378 (1993) .
17. R. S. Kern, L. B. Rowland, S. Tanaka, R. F. Davis, "Solid solutions of AlN and SiC grown by plasma-assisted, gas-source molecular beam epitaxy," J. Mat. Res.
18. Y. Xu, A. Zangvil, M. Landon, F. Thevenot, J. Am. Ceram. Soc. **75** [2], 325-333 (1992).
19. R. Ruh, A. Zangvil, J. Barlowe, Am. Ceram. Soc. Bull., **64** [10], 1368-1373 (1985).
20. L. L. Oden, R. A. McCune, J. Am. Ceram. Soc. **73** [6], 1529-1533 (1990).
21. R. J. Oscroft, D. P. Thompson, J. Am. Ceram. Soc. **74** [9], 2327-2328 (1991).
22. J. Chen, Q. Tian, A. V. Virkar, J. Am. Ceram. Soc. **75** [4], 809-821 (1992).
23. S. Y. Kuo, Z. C. Jou, A. V. Virkar, W. Rafaniello, J. Mat. Sci. **21**, 3019-3024 (1986).
24. C. L. Czekaj, M. Hackney, W. Hurley, L. Interrante, G. Sigel, P. Schields, G. Slack, J. Am. Ceram. Soc. **73** [2], 352-357 (1990).
25. A. Zangvil, R. Ruh, Silicon Carbide, 63-82 (1988).
26. A. Zangvil, R. Ruh, J. Am. Ceram. Soc. **71**[10], 884-890 (1988).
27. S. Kuo, A. V. Virkar, J. Am. Ceram. Soc. **72** [4], 540-550 (1989).
28. G. Sukhanek, Y. M. Tairov, V. F. Tsvetkov, Pis'ma Zh. Tekh. Fiz. **8** [12], 739-741 (1983).
29. N. B. Rafaevich, V. F. Tsvetkov, A. N. Komov, S. G. Losevskaya, Iz. Aka. Nauk SSSR, Neorg. Mater. **26** [5], 973-977, (1990).
30. M. M. Patience, P. J. England, D. P. Thompson , K. H. Jack, *Proc. of Inter. Sym. on Ceram. Components for Engine*, p. 473-479 (1983) Japan.

VI. Distribution List

	Number of Copies
Dr. Yoon Soo Park Office of Naval Research Applied Research Division Code 1212 800 N. Quincy Street Arlington, VA 22217-5000	3
Administrative Contracting Officer Office of Naval Research Resident Representative The Ohio State Univ. Research Ctr. 1960 Kenny Road Columbus, OH 43210-1063	1
Director Naval Research Laboratory ATTN: Code 2627 Washington, DC 20375	1
Defense Technical Information Center Bldg. 5, Cameron Station Alexandria, VA 22314	2